An Acceleration Method for AC Steady State Performance of Dual Three-phase Machine: Modeling and Implementation

1st Yu Li
College of electrical and information engineering
Hunan University
Changsha, China
liyu19900506@gmail.com

2nd Yaojing Feng
College of electrical and information engineering
Hunan University
Changsha, China
fengyaojing@hnu.edu.cn

3rd Shoudao Huang
College of electrical and information engineering
Hunan University
Changsha, China
hsd1962@hnu.edu.cn

4th Bo Ma
College of electrical and information engineering
Hunan University
Changsha, China
boma@hnu.edu.cn

5th Sa Zhu
College of Energy and Electrical Engineering
Hohai University
Nanjing, China
zhusa@hhu.edu.cn

6th Jianguo Zhu
School of Electrical and Information Engineering
Sydney University
NSW, Australia
jianguo.zhu@sydney.edu.au

2021 13th International Symposium on Linear Drives for Industry Applications (LDIA) | 978-1-7281-7210-1/21/$31.00 ©2021 IEEE | DOI: 10.1109/LDIA49489.2021.9505763

***Abstract*—This paper proposes a method to shorten the length of transient response time-stepping finite element analysis (TSFEA) of the dual three-phase permanent magnet synchronous machine (PMSM). Firstly, the initial magnetic potential and stator winding current under steady-state operation conditions in the TSFEA are estimated using time-harmonic finite element analysis (THFEA). Then the achieved relevant values extracted from the real and imaginary part in the time-harmonic solver are injected into a proposed zero-state govern equation called the "zero-state initial solver", which gives the closer-fitting of initial permeabilities, magnetic potential, and stator winding current in the time domain. Finally, the upper achieved values are transferred into the TSFEA as the initial condition for the following computation. With the well-precalculated solution, the required AC cycles of the steady-state can be effectively reduced, while the computing time of the central processing unit (CPU) is also substantially decreased. The effectiveness and accuracy of the proposed method are verified by comparing it with the conventional methods in a TSFEA of an 6-kW dual three-phase PMSM.**

Keywords—Dual three-phase machine, AC steady-state, time-harmonic finite element analysis, time-stepping finite element analysis.

I. INTRODUCTION

The versatility and powerfulness of time-stepping finite element method for the simulation of transient electromagnetic problems are well recognized. Typically, the slow steady-state convergence rarely exists in the transient simulation of a PMSM when the current source is applied since the stator electromagnetic time constant is directly eased. Nevertheless, the waveform of the current must be known before the simulation. The current distortion generally exists due to the current has abundant harmonic contents, which causes the waveform to be non-sinusoidal. If a machine is designed based only on the current-fed simulation, many unexpected troubles were exposed in the future; for example, torque ripples may not be accurately simulated. However, a more "physics-compliant" voltage supply suffered from a numerical fluctuation at the start of the simulation, which takes several periods to reach the AC steady-state [1-3].

Many methods have been proposed to overcome this problem in finite element analysis. One branch of them is known as the parallel computing technique, which aims to take advantage of the computational resource. For example, the time decomposition method (TDM)[4] and periodic parareal algorithm with initial-value coarse method [5]. The merits of upper mentioned methods are on reducing the simulation time while the numerical transient maintains the same as the conventional THFEA. However, the drawback is the high dependence on the performance of the computer.

Harmonic balance FEM can generate periodic steady-state solutions of nonlinear problems without time-stepping during the transient process by processing the magnetic field harmonics and magnetic material nonlinear characteristics simultaneously [6]. It usually reduces the total problem size with the cost of a denser system matrix, which means it will take longer to solve. The model order reduction technique can reduce a high order model to a lower order model and adjust the nonlinear iteration time-stepping error tolerance [7]. This method merits a low computational burden and quick transient, but the model reduction decreases the computational precision.

Another kind of technique is to reduce the time cost of numerical transient convergence time in TSFEA using the well-determined initial values achieved by THFEA[8]. In the relevant research in induction machines, it is also known as "virtual blocked rotor" (VBR) method [9]. This method was based on a time-harmonic solver in the frequency domain to approximate initial conditions. Nevertheless, this existing method does not take the full usage of THFEA on time-zero (t=0) condition estimation in the TSFEA. To be more specific, this method only extracted from the real part of the complex solution in THFEA into TSFEA, which includes magnetic potential and stator winding current. To accelerate the TSFEA further, an acceleration technique named as "zero-state initial solver" (ZSIS) is proposed in this papar. Different from the existing VBR method, the real and imaginary parts in THFEA are injected into the established

978-1-7281-7210-1/21/$31.00 ©2021 IEEE

zero states govern system to obtain a more accurate initial condition estimation with small calculation cost. With the obtained solution, the following convergence time of the TSFEA is effectively reduced.

For the complete introduction of the proposed method, the rest of this paper is organized as follows. In Section II, a general formulation of field-circuit coupling is presented, followed by its time-harmonic discretization in the frequency domain. The Taylor expansion on the nonanalytic equation system is performed for evaluating the derivatives before the presentation of the Newton process. Section III introduces the specific implementation of the proposed acceleration technique and the comparison of the traditional methods. Section IV presents the TSFEA of a dual three-phase PMSM as shown in Fig. 1 by the proposed method and the comparison results with the traditional methods, followed by the conclusion drawn in Section V.

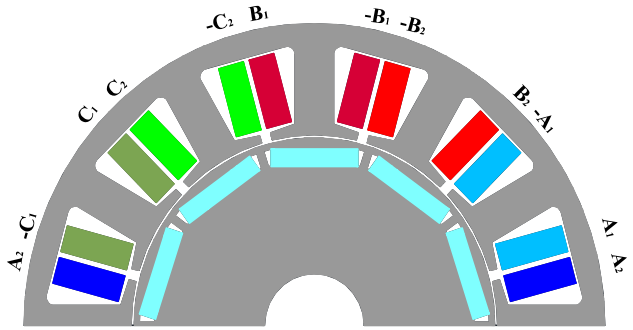

Fig. 1. Structure diagram

II. Detailed Modeling and Implementation

A. Field-circuit model of 2-D machine

With stranded winding coils, the eddy currents and proximity effects of the winding conductor region is not considered in this study. The current density of each stranded conductor is considered evenly distributed. The governing equation only considering the eddy effect in permanent magnet conductor can be expressed as follows

$$\nabla\times\boldsymbol{H}+\sigma_{pm}\frac{\partial\boldsymbol{A}}{\partial t}-\frac{\sigma_{pm}}{l_{ef}}\sum_{j=1}^{Q_{pm}}u_j^{pm}-\sum_{j=1}^{Q_s}\beta_j^s\frac{N_{str,j}}{\Delta_j}i_j^s=\nabla\times\boldsymbol{H}_c \tag{1}$$

where $\boldsymbol{H}$ is the magnetic field intensity, $\boldsymbol{A}$ the magnetic potential, u_j^{pm} the scalar potential difference in the j-th PM conductor, σ_{pm} the material conductivity, Q_{pm} the number of PM in the solution region, Q_s the number of stranded conductors in the solution region, i_j^s the current in the j-th stranded conductor, $\boldsymbol{H_c}$ the magnetic coercivity, β_j^s the parameter of correspondence between the field point and the j-th stranded conductor, and

$$\beta_j^s=\begin{cases}1 & \text{points on positively oriented strands of conductor } j\\ -1 & \text{points on negatively oriented strands of conductor } j\\ 0 & \text{otherwise}\end{cases}$$

The model should also include following circuit equations:

$$R_j^{pm}\sigma_{pm}\int_{\Omega_{pm}}\frac{\partial\boldsymbol{A}}{\partial t}d\Omega-u_j^{pm}=0 \tag{2}$$

$$l_{ef}\int_{\boldsymbol{\Omega}_s}\frac{N_{str,j}}{\boldsymbol{\Delta}_j}\frac{\partial\boldsymbol{A}}{\partial t}d\Omega+R_j^s i_j^s=u_j^s \tag{3}$$

$$\sum_{j=1}^{Q_s}\pm u_j^s+\sum_{j=1}^{Q_s}\pm(R_j^{ew}+L_j^{ew}\frac{d}{dt})i_j^s=\boldsymbol{U}_{supply} \tag{4}$$

where $N_{str,j}$ is the number of turns, Δ_j the cross-section, $R_j^s=\left(N_{str,j}^2 l_{ef}\right)/\left(\sigma f_{str}\Delta_j\right)$ the DC resistance, u_j^s the voltage drops, R_j^{ew} and L_j^{ew} are the end winding DC resistance and inductance of the j-th stranded conductor, respectively, l_{ef} is the effective length of the machine, f_{str} the fill factor of the stranded conductor, σ the stranded material conductivity and $\boldsymbol{U}_{supply}$ the external circuit with supply source, $\Omega_{pm,}$ and Ω_s are domains of PM conductor region and stranded conductor region, respectively.

B. Time-harmonic discretization

Assuming a purely sinusoidal behavior, the time dependence can be eliminated from the equations by using complex field quantities. In a 2D case, applying the Galerkin's method to equations (1)-(4) with the shape function N, one obtains:

$$0=F_i^a(\overline{H},\bar{a},\overline{u^{pm}},\bar{i}^s)=\int\left(N_i\cdot\nabla\times\overline{\boldsymbol{H}}\right)d\Omega+\mathrm{j}\omega\cdot\sigma_{pm}\int(N_i\cdot N_j\cdot\bar{a}_j)d\Omega-$$
$$\frac{\sigma_{pm}}{l_{ef}}\int(N_i\cdot\sum_{j=1}^{Q_{pm}}\overline{u_j^{pm}})d\Omega-\int\left(N_i\cdot\sum_{j=1}^{Q_s}\frac{N_{str,j}}{\Delta_j}\beta_j^s\bar{i}_j^s\right)d\Omega-\int\left(\boldsymbol{H}_c\cdot\nabla\times\boldsymbol{N}_i\right)d\Omega \tag{5}$$

$$0=F_i^b(\bar{a},\overline{u^{pm}})=\mathrm{j}\omega R_i^{pm}\int\left(\sigma_{pm}N_i\cdot\bar{a}_i\right)d\Omega-\overline{u_i^{pm}} \tag{6}$$

$$0=F_i^c(\bar{a},\bar{i}^s)=\sum_{j=1}^{Q_s}\pm\left\{\mathrm{j}\omega l_{ef}\int\left(\frac{N_{str,j}}{\Delta_j}N_i\bar{a}_i\right)d\Omega\right.$$
$$\left.+(R_j^s+R_j^{ew}+\mathrm{j}\omega L_j^{ew})\bar{i}_j^s\right\}-\boldsymbol{U}_{supply} \tag{7}$$

where $\overline{\boldsymbol{H}}$ is the complex vector of magnetic field intensity, $\overline{\boldsymbol{u^{pm}}}$ the complex vector of potential difference, $\bar{\boldsymbol{a}}$ the nodal value of complex magnetic potential, and $\bar{\boldsymbol{i}}^s$ the complex vector of stranded conductor currents.

The complex system of equations can be rewritten in the matrix form as

$$\left(\boldsymbol{F}^a\right)^{\mathrm{R}}=\int N_i\cdot\nabla\times\left(\overline{\boldsymbol{H}}\right)^{\mathrm{R}}d\Omega-\omega\boldsymbol{M}\cdot\left(\bar{\boldsymbol{a}}\right)^{\mathrm{I}}-\frac{1}{l_{ef}}\boldsymbol{C}\cdot\left(\overline{\boldsymbol{u}^{pm}}\right)^{\mathrm{R}}-\boldsymbol{G}\cdot\left(\bar{\boldsymbol{i}}^s\right)^{\mathrm{R}}-\boldsymbol{P} \tag{8}$$

$$\left(\boldsymbol{F}^b\right)^{\mathrm{R}}=-\omega\boldsymbol{R}^{pm}\cdot\boldsymbol{C}^T\cdot\left(\bar{\boldsymbol{a}}\right)^{\mathrm{I}}-\left(\boldsymbol{u}^{pm}\right)^{\mathrm{R}} \tag{9}$$

$$\left(\boldsymbol{F}^c\right)^{\mathrm{R}}=-\omega l_{ef}\boldsymbol{G}^T\cdot\left(\bar{\boldsymbol{a}}\right)^{\mathrm{I}}+\boldsymbol{R}\cdot\left(\bar{\boldsymbol{i}}^s\right)^{\mathrm{R}}-\omega\boldsymbol{L}\cdot\left(\bar{\boldsymbol{i}}^s\right)^{\mathrm{I}}-\left(\boldsymbol{U}_{supply}\right)^{\mathrm{R}} \tag{10}$$

$$\left(\boldsymbol{F}^a\right)^{\mathrm{I}}=\int N_i\cdot\nabla\times\left(\overline{\boldsymbol{H}}\right)^{\mathrm{I}}d\Omega+\omega\boldsymbol{M}\cdot\left(\bar{\boldsymbol{a}}\right)^{\mathrm{R}}-\frac{1}{l_{ef}}\boldsymbol{C}\cdot\left(\overline{\boldsymbol{u}^{pm}}\right)^{\mathrm{I}}-\boldsymbol{G}\cdot\left(\bar{\boldsymbol{i}}^s\right)^{\mathrm{I}}-\boldsymbol{P} \tag{11}$$

$$\left(\boldsymbol{F}^b\right)^{\mathrm{I}}=\omega\boldsymbol{R}^{pm}\cdot\boldsymbol{C}^T\cdot\left(\bar{\boldsymbol{a}}\right)^{\mathrm{R}}-\left(\boldsymbol{u}^{pm}\right)^{\mathrm{I}} \tag{12}$$

$$\left(\boldsymbol{F}^c\right)^{\mathrm{I}}=\omega l_{ef}\boldsymbol{G}^T\cdot\left(\bar{\boldsymbol{a}}\right)^{\mathrm{R}}+\boldsymbol{R}\cdot\left(\bar{\boldsymbol{i}}^s\right)^{\mathrm{I}}+\omega\boldsymbol{L}\cdot\left(\bar{\boldsymbol{i}}^s\right)^{\mathrm{R}}-\left(\boldsymbol{U}_{supply}\right)^{\mathrm{I}} \tag{13}$$

The dimensions of the matrices and their elements are:

$$[\boldsymbol{G}]_{Q_n\times Q_m},\quad G_{ij}=\int_{\Omega}N_i\sum_{j=1}^{Q_s}\frac{N_{str,j}}{\Delta_j}\beta_j^s d\Omega=\left(G_{ji}\right)^T,$$

$$[\boldsymbol{M}]_{Q_n\times Q_n},\quad M_{ij}=\int\sigma^{pm}N_iN_j d\Omega,$$

$$\left[\boldsymbol{C}\right]_{Q_n\times Q_{pm}},\ C_{ij}=\int \sigma^{pm}N_i d\Omega=(C_{ji})^T,$$

$$\left[\boldsymbol{R}\right]_{Q_m\times Q_s},\ R_{ij}=\left(\beta_i^s\right)^T\cdot\sum_{j=1}^{Q_s}\left[\left(R_j^s+R_j^{ew}\right)\right],$$

$$\left[\boldsymbol{R}^{pm}\right]_{Q_{pm}\times Q_{pm}},\ R_{ij}^{pm}=\mathrm{diag}(l_{ef}/(\sigma_{pm}\cdot S_{pm}))$$

$$\left[\boldsymbol{L}\right]_{Q_m\times Q_s},\ L_{ij}=\left(\beta_i^s\right)^T\cdot\sum_{j=1}^{Q_s}\left[L_j^{ew}\right],$$

$$\left[\boldsymbol{P}\right]_{Q_n\times 1},\ P_i=\int\left(\boldsymbol{H}_c\cdot\nabla\times\boldsymbol{N}_i\right)d\Omega,$$

$$\left[\boldsymbol{U}_{supply}\right]_{Q_m\times 1},\text{and}$$

$$U_{supply}=[U\,\mathrm{e}^{\mathrm{j}(\omega t-\varphi)},U\,\mathrm{e}^{\mathrm{j}(\omega t-\varphi-\pi/6)},U\,\mathrm{e}^{\mathrm{j}(\omega t-\varphi-2\pi/3)},$$
$$U\,\mathrm{e}^{\mathrm{j}(\omega t-\varphi-5\pi/6)},U\,\mathrm{e}^{\mathrm{j}(\omega t-\varphi-4\pi/3)},U\,\mathrm{e}^{\mathrm{j}(\omega t-\varphi-3\pi/2)}]^T$$

where Q_n is the number of nodal potentials, Q_m the number of phases, ω the angular velocity, φ the power factor angle, U the line voltage amplitude, t time, ω the angular velocity, and superscripts R and I denote the real and imaginary components of a vector or matrix.

C. Taylor expansion and evaluation of derivatives

As mentioned above, the time-harmonic discretization systems (8) and (11) are not analytical because they do not follow the Cauchy-Riemann differential equations. Consequently, the Taylor expansion is applied to (8) and (11), and we obtain

$$\left(\boldsymbol{F}^a\right)^{\mathrm{R}}+\sum_{j=1}^{Q_n}\left(\frac{\partial\left(\boldsymbol{F}^a\right)^{\mathrm{R}}}{\partial\left(\overline{a}_j\right)^{\mathrm{R}}}\cdot\Delta\left(\overline{a}_j\right)^{\mathrm{R}}+\frac{\partial\left(\boldsymbol{F}^a\right)^{\mathrm{R}}}{\partial\left(\overline{a}_j\right)^{\mathrm{I}}}\cdot\Delta\left(\overline{a}_j\right)^{\mathrm{I}}\right)=0 \quad (14)$$

$$\left(\boldsymbol{F}^a\right)^{\mathrm{I}}+\sum_{j=1}^{Q_n}\left(\frac{\partial\left(\boldsymbol{F}^a\right)^{\mathrm{I}}}{\partial\left(\overline{a}_j\right)^{\mathrm{R}}}\cdot\Delta\left(\overline{a}_j\right)^{\mathrm{R}}+\frac{\partial\left(\boldsymbol{F}^a\right)^{\mathrm{I}}}{\partial\left(\overline{a}_j\right)^{\mathrm{I}}}\cdot\Delta\left(\overline{a}_j\right)^{\mathrm{I}}\right)=0 \quad (15)$$

Taking partial derivatives of (14) and (15), one obtains

$$\frac{\partial\left(\boldsymbol{F}^a\right)^{\mathrm{R}}}{\partial\left(\overline{a}_j\right)^{\mathrm{R}}}=\int\left(\nabla\times N_i\right)\cdot\left(\frac{\partial\left(\overline{\boldsymbol{H}}\right)^{\mathrm{R}}}{\partial\left(\overline{\boldsymbol{B}}\right)^{\mathrm{R}}}\cdot\nabla\times N_j\right)d\Omega \quad (16)$$

$$\frac{\partial\left(\boldsymbol{F}^a\right)^{\mathrm{R}}}{\partial\left(\overline{a}_j\right)^{\mathrm{I}}}=\int\left(\nabla\times N_i\right)\cdot\left(\frac{\partial\left(\overline{\boldsymbol{H}}\right)^{\mathrm{R}}}{\partial\left(\overline{\boldsymbol{B}}\right)^{\mathrm{I}}}\cdot\nabla\times N_j\right)d\Omega-\omega\boldsymbol{M} \quad (17)$$

$$\frac{\partial\left(\boldsymbol{F}^a\right)^{\mathrm{I}}}{\partial\left(\overline{a}_j\right)^{\mathrm{R}}}=\int\left(\nabla\times N_i\right)\cdot\left(\frac{\partial\left(\overline{\boldsymbol{H}}\right)^{\mathrm{I}}}{\partial\left(\overline{\boldsymbol{B}}\right)^{\mathrm{R}}}\cdot\nabla\times N_j\right)d\Omega+\omega\boldsymbol{M} \quad (18)$$

$$\frac{\partial\left(\boldsymbol{F}^a\right)^{\mathrm{I}}}{\partial\left(\overline{a}_j\right)^{\mathrm{I}}}=\int\left(\nabla\times N_i\right)\cdot\left(\frac{\partial\left(\overline{\boldsymbol{H}}\right)^{\mathrm{I}}}{\partial\left(\overline{\boldsymbol{B}}\right)^{\mathrm{I}}}\cdot\nabla\times N_j\right)d\Omega \quad (19)$$

where $\left(\overline{\boldsymbol{B}}\right)^{\mathrm{R}}=\nabla\times\left(\overline{\boldsymbol{A}}\right)^{\mathrm{R}}=\sum_{k=1}^{Q_n}\left(\overline{a}_k\right)^{\mathrm{R}}\cdot\nabla\times N_k$

$$\left(\overline{\boldsymbol{B}}\right)^{\mathrm{I}}=\nabla\times\left(\overline{\boldsymbol{A}}\right)^{\mathrm{I}}=\sum_{k=1}^{Q_n}\left(\overline{a}_k\right)^{\mathrm{I}}\cdot\nabla\times N_k$$

The detailed derivation of complex reluctivity tensors, $\partial(\overline{\boldsymbol{H}})^{\mathrm{R}}/\partial(\overline{\boldsymbol{B}})^{\mathrm{R}}$, $\partial(\overline{\boldsymbol{H}})^{\mathrm{R}}/\partial(\overline{\boldsymbol{B}})^{\mathrm{I}}$, $\partial(\overline{\boldsymbol{H}})^{\mathrm{I}}/\partial(\overline{\boldsymbol{B}})^{\mathrm{R}}$, and $\partial(\overline{\boldsymbol{H}})^{\mathrm{I}}/\partial(\overline{\boldsymbol{B}})^{\mathrm{I}}$, are presented in the Appendix.

D. Newton's method processes

Because of nonlinearity, the complex field-circuit equations, (8)–(13), should be solved iteratively. The real and imaginary parts are the partition, and Newton's method is applied. The complex Jacobian matrix in the nonlinear magnetic material is given in Section II.C. The correction vector at the k-th iteration step can be obtained by solving

$$\begin{bmatrix}\left[\mathbf{J}^{aa}\right]^k & -\frac{1}{l_{ef}}\boldsymbol{C} & -\boldsymbol{G}\\ 0 & -\mathbf{I} & 0\\ 0 & 0 & \boldsymbol{R}\\ \left[\mathbf{J}^{ba}\right]^k+\omega\boldsymbol{M} & 0 & 0\\ \omega\boldsymbol{R}^{pm}\cdot\boldsymbol{C}^T & 0 & 0\\ \omega l_{ef}\boldsymbol{G}^T & 0 & \omega\boldsymbol{L}\end{bmatrix}$$

$$\begin{bmatrix}\left[\mathbf{J}^{ab}\right]^k-\omega\boldsymbol{M} & 0 & 0\\ -\omega\boldsymbol{R}^{pm}\cdot\boldsymbol{C}^T & 0 & 0\\ -\omega l_{ef}\boldsymbol{G}^T & 0 & -\omega\boldsymbol{L}\\ \left[\mathbf{J}^{bb}\right]^k & -\frac{1}{l_{ef}}\boldsymbol{C} & -\boldsymbol{G}\\ 0 & -\mathbf{I} & 0\\ 0 & 0 & \boldsymbol{R}\end{bmatrix}\times\begin{bmatrix}\Delta\left(\overline{\boldsymbol{a}}\right)^{\mathrm{R}}\\ \Delta\left(\overline{\boldsymbol{u}^{pm}}\right)^{\mathrm{R}}\\ \Delta\left(\overline{\boldsymbol{i}^s}\right)^{\mathrm{R}}\\ \Delta\left(\overline{\boldsymbol{a}}\right)^{\mathrm{I}}\\ \Delta\left(\overline{\boldsymbol{u}^{pm}}\right)^{\mathrm{I}}\\ \Delta\left(\overline{\boldsymbol{i}^s}\right)^{\mathrm{I}}\end{bmatrix}^{(k)}=\begin{bmatrix}-\left(\boldsymbol{F}^a\right)^{\mathrm{R}}\\ \left(\boldsymbol{F}^b\right)^{\mathrm{R}}\\ \left(\boldsymbol{F}^c\right)^{\mathrm{R}}\\ -\left(\boldsymbol{F}^a\right)^{\mathrm{I}}\\ \left(\boldsymbol{F}^b\right)^{\mathrm{I}}\\ \left(\boldsymbol{F}^c\right)^{\mathrm{I}}\end{bmatrix} \quad (20)$$

where $\mathbf{I}$ is an Identity matrix

$$\left[\mathbf{J}^{aa}\right]_{Q_n\times Q_n},\ \mathrm{J}_{ij}^{aa}=\int\left(\nabla\times N_i\right)\cdot\left(\frac{\partial\left(\overline{\boldsymbol{H}}\right)^{\mathrm{R}}}{\partial\left(\overline{\boldsymbol{B}}\right)^{\mathrm{R}}}\cdot\nabla\times N_j\right)d\Omega$$

$$\left[\mathbf{J}^{ab}\right]_{Q_n\times Q_n},\ \mathrm{J}_{ij}^{ab}=\int\left(\nabla\times N_i\right)\cdot\left(\frac{\partial\left(\overline{\boldsymbol{H}}\right)^{\mathrm{R}}}{\partial\left(\overline{\boldsymbol{B}}\right)^{\mathrm{I}}}\cdot\nabla\times N_j\right)d\Omega$$

$$\left[\mathbf{J}^{ba}\right]_{Q_n\times Q_n},\ \mathrm{J}_{ij}^{ba}=\int\left(\nabla\times N_i\right)\cdot\left(\frac{\partial\left(\overline{\boldsymbol{H}}\right)^{\mathrm{I}}}{\partial\left(\overline{\boldsymbol{B}}\right)^{\mathrm{R}}}\cdot\nabla\times N_j\right)d\Omega$$

$$\left[\mathbf{J}^{bb}\right]_{Q_n\times Q_n},\ \mathrm{J}_{ij}^{bb}=\int\left(\nabla\times N_i\right)\cdot\left(\frac{\partial\left(\overline{\boldsymbol{H}}\right)^{\mathrm{I}}}{\partial\left(\overline{\boldsymbol{B}}\right)^{\mathrm{I}}}\cdot\nabla\times N_j\right)d\Omega.$$

The coefficient matrix of equation system (20) consists of four $(Q_n+Q_{pm}+Q_m)\times(Q_n+Q_{pm}+Q_m)$ nonsymmetric sparse submatrices. By solving (20), the convergence to steady-state can be achieved iteratively.

III. Acceleration Methods

As outlined above, the magnetic potentials can be obtained from the system (20). In the time-harmonic analysis, magnetic potential $\boldsymbol{a}$ can be described as a periodic function shown below:

$$\boldsymbol{a}(t)=\left(\bar{\boldsymbol{a}}\right)^{\mathrm{R}}\cdot\cos(\omega t)-\left(\bar{\boldsymbol{a}}\right)^{\mathrm{I}}\cdot\sin(\omega t) \tag{21}$$

$$\boldsymbol{a}(0)=\left(\bar{\boldsymbol{a}}\right)^{\mathrm{R}},\boldsymbol{a}(0)=-\omega\left(\bar{\boldsymbol{a}}\right)^{\mathrm{I}} \tag{22}$$

Through the relation of time-domain and time-harmonic equation (21)-(22) at time zero, we inject into ZSIS to acquire an approximation of initial value for TSFEA. It concluded the zero-state govern equation in the time domain, expressed as

$$\begin{bmatrix}\boldsymbol{S} & -\dfrac{\boldsymbol{C}}{l_{ef}} & -\boldsymbol{G}\\ 0 & -\mathbf{I} & 0\\ 0 & 0 & \boldsymbol{R}\end{bmatrix}\times\begin{bmatrix}\boldsymbol{a}\\ \boldsymbol{u}^{pm}\\ \boldsymbol{i}^{s}\end{bmatrix}=\begin{bmatrix}\boldsymbol{P}+\omega\boldsymbol{M}\cdot(\bar{\boldsymbol{a}})^{\mathrm{I}}\\ \omega\boldsymbol{R}^{pm}\cdot\boldsymbol{C}^{T}\cdot(\bar{\boldsymbol{a}})^{\mathrm{I}}\\ \omega l_{ef}\boldsymbol{G}^{T}\cdot(\bar{\boldsymbol{a}})^{\mathrm{I}}+\omega\boldsymbol{L}\cdot(\bar{\boldsymbol{i}}^{s})^{\mathrm{I}}\end{bmatrix}\Bigg|_{t=0} \tag{23}$$

The zero states govern equation is solved by Newton Raphson method. The system (23) matrix right side includes nonlinear matrix $\boldsymbol{S}$ materials in stator and rotor cores, linear matrix term $\boldsymbol{C}$, $\boldsymbol{G}$. The system matrix left side includes magnetization vector $\boldsymbol{P}$, time-dependent term matrix $\boldsymbol{M}$, $\boldsymbol{C}^{\mathrm{T}}$, $\boldsymbol{G}^{T}$, and $\boldsymbol{L}$. The flow chart of the implementation of two method is shown in Fig. 2. In the red blank box, this method similar to VBR technique, the total system (20) is settled through nonlinear iteration in the frequency domain. Afterward, the real part of stator currents and magnetic potential is injected into the TSFEA in the time domain. In the blue blank box, the same step as the VBR method, the real part and imaginary part extract from THFEA. Meanwhile, the achieved real and imaginary parts of the solution from THFEA are transferred into the zero-state govern system (23). The real part is injected into the system (23) as the primal value, and then the imaginary part is used as the loaded term of the system (23) on the left side, which considers the influence of the eddy current effect. Afterward, the ZSIS takes few iterative steps to obtain an accurate approximation of the initial value for TSFEA, which includes the magnetic potential, stator current.

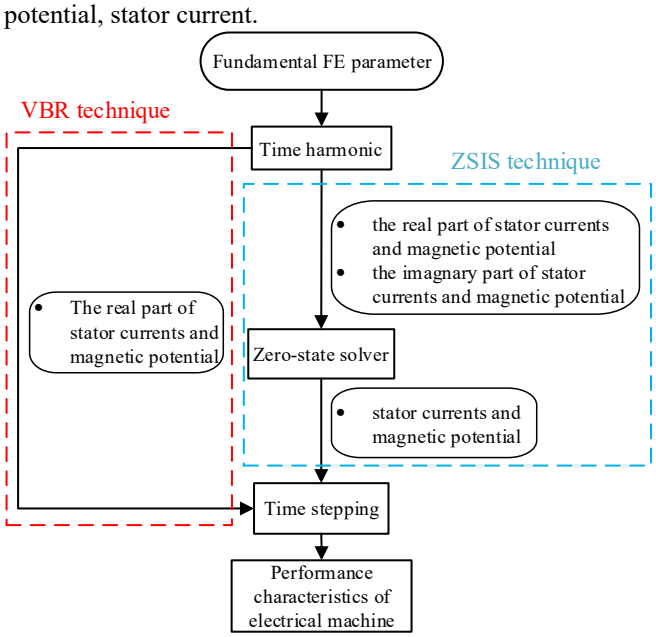

Fig. 2. Flow chart of implementation differences between the VBR and ZSIS methods

IV. Comparison of Simulation Results

The TSFEA of the 6-kw dual three-phase PMSM is conducted by the proposed technique, and both the conventional TSFEA method and VBR method are also applied for the comparison. The main machine parameters are listed in Table I. The simulation is performed with 100 time-steps per period, a relative residual norm of 10^{-5}, which is enough to ensure convergence. The mesh diagram is illustrated in Fig. 3, and the number of the triangular elements and degrees of freedom are 11703 and 6448, respectively. Both the proposed and conventional simulation models were run on Matlab in the same workstation with Intel Xeon E5-2678 CPU.

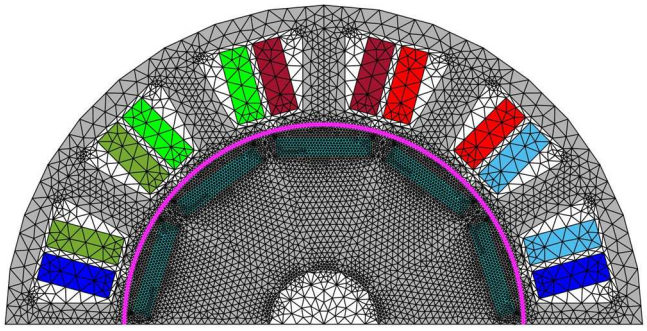

(a)

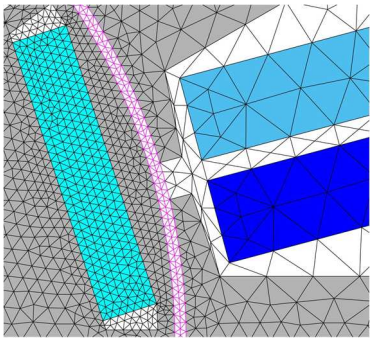

(b)

Fig. 3. Mesh diagram of the (a) half model, (b) zoom-in air gap.

TABLE I: Parameters of the 6-kw dual three-phase PMSM

Parameter	Value
Winding connection	Star
Number of parallel paths	2
Number of turns	57
Pole-arc	0.8
Number of stator slots	12
Number of poles	10
Air-gap length (mm)	1
Outer radius of stator (mm)	174
Inner radius of stator (mm)	110
Stack length (mm)	100
Rated torque (Nm)	20
Rated speed (r/min)	3000
Rated voltage (V)	175
Rated current (A)	12.27
Rated frequency (Hz)	250

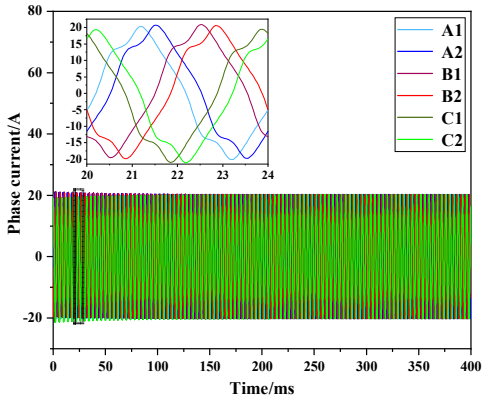

(a)

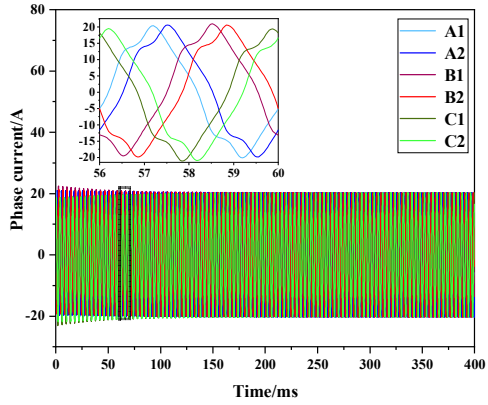

(b)

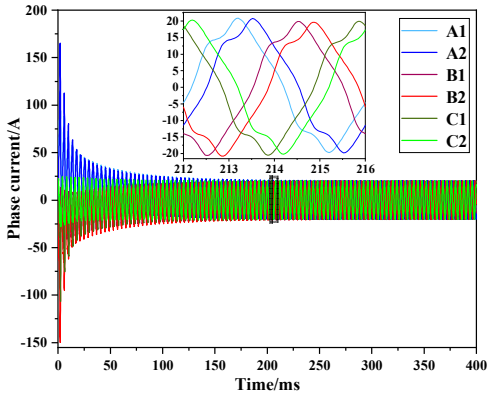

(c)

Fig. 5. Phase current waveforms were obtained by the (a) ZSIS method, (b) VBR method, and (c) conventional method.

The variation of the RMS value of each phase current in the electrical cycle is utilized to determine the steady-state is achieved. The specific differentials of the phase current between the adjacent electrical cycle is set as 0.2% for confirming the convergence.

Figs. 5 shows the waveforms of phase currents of the machine obtained by the proposed ZSIS method, VBR method, and conventional TSFEA methods, respectively. It should be noted that the transient response convergence at 20ms, 56ms, and 212ms respectively in the analysis by the three methods. The corresponding number of AC cycles are 5, 14, and 53. By contrast, the required cycles are decreased from 53 to 5, which means 90.57% improvement.

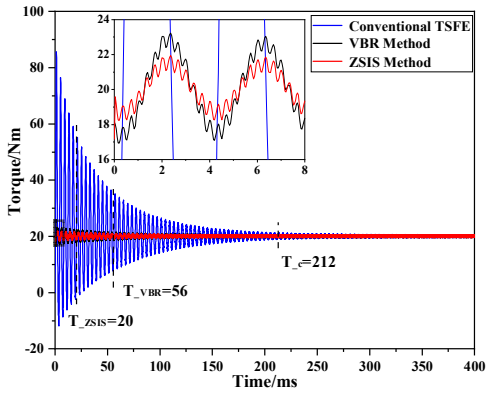

(a)

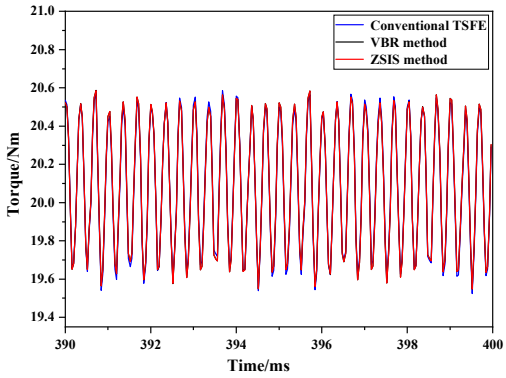

(b)

Fig. 6. Transient torque comparison in (a) the whole transient analysis process and (b) the time domain when all the calculation methods convergence.

Fig. 6(a) compares the simulated torque curves by the ZSIS method, VBR method, and traditional methods. The proposed method results have less fluctuation and fast convergence than the traditional method. The proposed method results have less fluctuation and fast convergence than the traditional method. It is noted that the ZSIS method is closer to the AC steady state at the beginning of the calculation than the VBR method. Fig.6(b) shows the good agreement between the steady-state torque results obtained by the proposed and traditional methods, demonstrating the excellent accuracy of the proposed method.

TABLE II
SIMULATION DETAILS

	ZSIS method	VBR method	Conventional
CPU time, (min)	6.47	11.01	40.11

Table II compares the convergence speed of the proposed and conventional methods. By contrast, the VBR method requires 27.45% of the CPU time of the traditional time-stepping method to reach the steady-state in the torque curve, while the ZSIS method is more economical than the previous one, only 16.13% of CPU time. The effectiveness of the well proved.

V. CONCLUSION

This paper proposes a ZSIS method to accelerate the convergence of the transient process in TSFEA for a dual three-phase PMSM. Compared to the traditional methods, the proposed methods can significantly reduce the CPU time and number of AC cycles required to reach the steady-state while

retaining the accuracy of the traditional TSFEA method. Since the proposed method is derived under very general conditions, it is applicable to other types of electrical machines.

ACKNOWLEDGMENT

The funding sponsorship was provided by The National Key Research and Development Program of China (2018YFB0606000).

APPENDIX. DERIVATION OF COMPLEX RELUCTIVITY TENSOR

The expression of complex reluctivity tensor can be derived from the 2D phasor expression of field vector, which bears an elliptical hysteresis loop, as the following

$$\left(\overline{\boldsymbol{H}}\right)^{\mathrm{R}} = v_{ref}\cdot\left(\overline{\boldsymbol{B}}\right)^{\mathrm{R}} = v_{ref}\cdot\left[\mathbf{i}(\overline{B}_x)^{\mathrm{R}} + \mathbf{j}(\overline{B}_y)^{\mathrm{R}}\right] \tag{21}$$

$$\left(\overline{\boldsymbol{H}}\right)^{\mathrm{I}} = v_{ref}\cdot\left(\overline{\boldsymbol{B}}\right)^{\mathrm{I}} = v_{ref}\cdot\left[\mathbf{i}(\overline{B}_x)^{\mathrm{I}} + \mathbf{j}(\overline{B}_y)^{\mathrm{I}}\right] \tag{22}$$

$$\overline{\boldsymbol{B}}^2 = \left[(\overline{B}_x)^{\mathrm{R}}\right]^2 + \left[(\overline{B}_y)^{\mathrm{R}}\right]^2 + \left[(\overline{B}_x)^{\mathrm{I}}\right]^2 + \left[(\overline{B}_y)^{\mathrm{I}}\right]^2 \tag{23}$$

Taking partial derivatives of field strength, one obtains

$$\frac{\partial\left(\overline{\boldsymbol{H}}\right)^{\mathrm{R}}}{\partial\left(\overline{\boldsymbol{B}}\right)^{\mathrm{R}}} = \begin{bmatrix} \dfrac{\partial(\overline{H}_x)^{\mathrm{R}}}{\partial(\overline{B}_x)^{\mathrm{R}}} & \dfrac{\partial(\overline{H}_x)^{\mathrm{R}}}{\partial(\overline{B}_y)^{\mathrm{R}}} \\ \dfrac{\partial(\overline{H}_y)^{\mathrm{R}}}{\partial(\overline{B}_x)^{\mathrm{R}}} & \dfrac{\partial(\overline{H}_y)^{\mathrm{R}}}{\partial(\overline{B}_y)^{\mathrm{R}}} \end{bmatrix} \tag{24}$$

$$\frac{\partial\left(\overline{\boldsymbol{H}}\right)^{\mathrm{R}}}{\partial\left(\overline{\boldsymbol{B}}\right)^{\mathrm{I}}} = \begin{bmatrix} \dfrac{\partial(\overline{H}_x)^{\mathrm{R}}}{\partial(\overline{B}_x)^{\mathrm{I}}} & \dfrac{\partial(\overline{H}_x)^{\mathrm{R}}}{\partial(\overline{B}_y)^{\mathrm{I}}} \\ \dfrac{\partial(\overline{H}_y)^{\mathrm{R}}}{\partial(\overline{B}_x)^{\mathrm{I}}} & \dfrac{\partial(\overline{H}_y)^{\mathrm{R}}}{\partial(\overline{B}_y)^{\mathrm{I}}} \end{bmatrix} = \frac{\partial\left(\overline{\boldsymbol{H}}\right)^{\mathrm{I}}}{\partial\left(\overline{\boldsymbol{B}}\right)^{\mathrm{R}}} \tag{25}$$

$$\frac{\partial\left(\overline{\boldsymbol{H}}\right)^{\mathrm{I}}}{\partial\left(\overline{\boldsymbol{B}}\right)^{\mathrm{I}}} = \begin{bmatrix} \dfrac{\partial(\overline{H}_x)^{\mathrm{I}}}{\partial(\overline{B}_x)^{\mathrm{I}}} & \dfrac{\partial(\overline{H}_x)^{\mathrm{I}}}{\partial(\overline{B}_y)^{\mathrm{I}}} \\ \dfrac{\partial(\overline{H}_y)^{\mathrm{I}}}{\partial(\overline{B}_x)^{\mathrm{I}}} & \dfrac{\partial(\overline{H}_y)^{\mathrm{I}}}{\partial(\overline{B}_y)^{\mathrm{I}}} \end{bmatrix} \tag{26}$$

where

$$\frac{\partial(\overline{H}_x)^{\mathrm{R}}}{\partial(\overline{B}_x)^{\mathrm{R}}} = \frac{\partial}{\partial(\overline{B}_x)^{\mathrm{R}}}[v_{ref}(\overline{\boldsymbol{B}}^2)\cdot(\overline{B}_x)^{\mathrm{R}}] = v_{ref} + 2\frac{\partial v_{ref}}{\partial\overline{\boldsymbol{B}}^2}\cdot(\overline{B}_x)^{\mathrm{R}}\cdot(\overline{B}_x)^{\mathrm{R}}$$

$$\frac{\partial(\overline{H}_y)^{\mathrm{R}}}{\partial(\overline{B}_x)^{\mathrm{R}}} = \frac{\partial(\overline{H}_x)^{\mathrm{R}}}{\partial(\overline{B}_y)^{\mathrm{R}}} = \frac{\partial}{\partial(\overline{B}_y)^{\mathrm{R}}}[v_{ref}(\overline{\boldsymbol{B}}^2)\cdot(\overline{B}_x)^{\mathrm{R}}] = 2\frac{\partial v_{ref}}{\partial\overline{\boldsymbol{B}}^2}\cdot(\overline{B}_y)^{\mathrm{R}}\cdot(\overline{B}_x)^{\mathrm{R}}$$

$$\frac{\partial(\overline{H}_y)^{\mathrm{R}}}{\partial(\overline{B}_y)^{\mathrm{R}}} = \frac{\partial}{\partial(\overline{B}_y)^{\mathrm{R}}}[v_{ref}(\overline{\boldsymbol{B}}^2)\cdot(\overline{B}_y)^{\mathrm{R}}] = v_{ref} + 2\frac{\partial v_{ref}}{\partial\overline{\boldsymbol{B}}^2}\cdot(\overline{B}_y)^{\mathrm{R}}\cdot(\overline{B}_y)^{\mathrm{R}}$$

$$\frac{\partial(\overline{H}_y)^{\mathrm{R}}}{\partial(\overline{B}_x)^{\mathrm{I}}} = \frac{\partial}{\partial(\overline{B}_x)^{\mathrm{I}}}[v_{ref}(\overline{\boldsymbol{B}}^2)\cdot(\overline{B}_x)^{\mathrm{R}}] = 2\frac{\partial v_{ref}}{\partial\overline{\boldsymbol{B}}^2}\cdot(\overline{B}_x)^{\mathrm{I}}\cdot(\overline{B}_x)^{\mathrm{R}}$$

$$\frac{\partial(\overline{H}_x)^{\mathrm{R}}}{\partial(\overline{B}_y)^{\mathrm{I}}} = \frac{\partial}{\partial(\overline{B}_y)^{\mathrm{I}}}[v_{ref}(\overline{\boldsymbol{B}}^2)\cdot(\overline{B}_x)^{\mathrm{R}}] = 2\frac{\partial v_{ref}}{\partial\overline{\boldsymbol{B}}^2}\cdot(\overline{B}_y)^{\mathrm{I}}\cdot(\overline{B}_x)^{\mathrm{R}}$$

$$\frac{\partial(\overline{H}_y)^{\mathrm{R}}}{\partial(\overline{B}_y)^{\mathrm{I}}} = \frac{\partial}{\partial(\overline{B}_y)^{\mathrm{I}}}[v_{ref}(\overline{\boldsymbol{B}}^2)\cdot(\overline{B}_y)^{\mathrm{R}}] = 2\frac{\partial v_{ref}}{\partial\overline{\boldsymbol{B}}^2}\cdot(\overline{B}_y)^{\mathrm{I}}\cdot(\overline{B}_y)^{\mathrm{R}}$$

$$\frac{\partial(\overline{H}_x)^{\mathrm{I}}}{\partial(\overline{B}_x)^{\mathrm{I}}} = \frac{\partial}{\partial(\overline{B}_x)^{\mathrm{I}}}[v_{ref}(\overline{\boldsymbol{B}}^2)\cdot(\overline{B}_x)^{\mathrm{I}}] = v_{ref} + 2\frac{\partial v_{ref}}{\partial\overline{\boldsymbol{B}}^2}\cdot(\overline{B}_x)^{\mathrm{I}}\cdot(\overline{B}_x)^{\mathrm{I}}$$

$$\frac{\partial(\overline{H}_y)^{\mathrm{I}}}{\partial(\overline{B}_x)^{\mathrm{I}}} = \frac{\partial(\overline{H}_x)^{\mathrm{I}}}{\partial(\overline{B}_y)^{\mathrm{I}}} = \frac{\partial}{\partial(\overline{B}_y)^{\mathrm{I}}}[v_{ref}(\overline{\boldsymbol{B}}^2)\cdot(\overline{B}_x)^{\mathrm{I}}] = 2\frac{\partial v_{ref}}{\partial\overline{\boldsymbol{B}}^2}\cdot(\overline{B}_y)^{\mathrm{I}}\cdot(\overline{B}_x)^{\mathrm{I}}$$

$$\frac{\partial(\overline{H}_y)^{\mathrm{I}}}{\partial(\overline{B}_y)^{\mathrm{I}}} = \frac{\partial}{\partial(\overline{B}_y)^{\mathrm{I}}}[v_{ref}(\overline{\boldsymbol{B}}^2)\cdot(\overline{B}_y)^{\mathrm{I}}] = v_{ref} + 2\frac{\partial v_{ref}}{\partial\overline{\boldsymbol{B}}^2}\cdot(\overline{B}_y)^{\mathrm{I}}\cdot(\overline{B}_y)^{\mathrm{I}}$$

and partial derivative, $\partial v_{ref}/\partial\overline{\boldsymbol{B}}^2$ can be deduced from the magnetization curve.

REFERENCES

[1] C. Di, I. Petrov, J. Pyrhronen, J. Chen, " Accelerating the time-stepping finite-element analysis of induction machines in transient-magnetic solutions," *IEEE Access*., vol.7, no.5, pp. 2169-3536, 2019.

[2] T. Garbiec, "Fast computation of performance characteristi cs for solid-rotor induction motors with electrically inhomogeneous rotors," *IEEE Trans. Energy Convers.* , vol. 31, no. 4, pp. 1688–1696, 2016.

[3] M.A. Jabbar, et al. "Modeling and numerical simulation of a brushless permanent-magnet DC motor in dynamic conditions by time-stepping technique," *IEEE Trans. Ind. Appli.*, vol.40, no.4,pp.763-770,2004.

[4] Rosu, Marius, et al. "Multiphysics simulation by design for electrical machines, power electronics and dirves," John Wiley & Sons, 2017.

[5] Bast, D., et al. "Accelerated steady-state torque computation for induction machines using parallel-in-time algorithms." *IEEE Trans. Magn*., vol. 56, no. 2, pp. 8100209, 2020.

[6] O. Bíró, G. Koczka, and K. Preis, "Finite element solution of nonlinear eddy current problems with periodic excitation and its industrial applications,"*Applied Numerical Mathematics*., vol. 79,pp. 3–17, 2014.

[7] W. Fu, S. L. Ho, and P. Zhou, "Reduction of computing time for steady-state solutions of magnetic field and circuit coupled problems using time-domain finite-element method," *IEEE Trans. Magn*., vol. 48, no. 11, pp. 3363–3366, 2012.

[8] H. N. Koti, et al. "On shortening the numerical transient in time-stepping finite element analysis of induction motors: method implementation," in *Proc. IEEE Int. Elect. Mach. Drives Conf.* , May 12-15, pp.1157–1162, 2019.

[9] Chen, H. , et al. "Fast steady-state analysis in time-ttepping finite element simulation of induction motors based on virtual blocked rotor techniques," *IEEE Trans. Ind. Appli.*, vol. 56 no.4, pp.3731-3743. 2020.